Iraqi National Journal of Earth Science

www.earth.uomosul.edu.iq

Spatio-temporal Assessment and Prediction of Land Surface Temperature (LST) Dynamics of Kirkuk City Using GIS Techniques

Sumaya Falih Hasan[1], Mustafa Raad Hameed [2], Banaz Adib Fatah [3], Muntadher Aidi Shareef [*4]

[1,3,4] *Department of Surveying Engineering, Technical College- Kirkuk/ Northern Technical University, Mosul, Iraq.*

[2] *School Buildings Department, the General Directorate of Education, Babylon, Iraq.*

Article information

Received: 20- Nov -2024

Revised: 15- Feb -2025

Accepted: 19- May -2025

Available online: 01- Apr -2026

Keywords:
LST,
NDVI,
GIS,
Vegetation Cover,

Correspondence:
Name: Muntadher Aidi Shareef

Email: muntadher.a.shareef@ntu.edu.iq

ABSTRACT

Over the past few decades, the Kirkuk region in Iraq has been seriously threatened by global warming under climate and temperature change scenarios. Over the course of a year, the study examines the spatio-temporal fluctuations in Land Surface Temperature (LST) and how they affect the vegetation cover in Kirkuk, Iraq, for the period from January 1, 2019, to December 31, 2019. Utilizing satellite data and Geographic Information Systems (GIS) techniques, the study analyzed the correlation between LST and the Normalized Difference Vegetation Index (NDVI), showing a fair but negative correlation (R^2 = 0.65). Additionally, the relationship between NDVI and Kirkuk wheat yield indicated a strong positive correlation (R^2 = 0.89). The results reveal that factors such as urban expansion, changes in cropping patterns, and global climate change contribute to the increase in LST. The findings highlight the importance of using remote sensing and GIS tools to assess climatic influences on environmental conditions, which are essential for sustainable land management and agricultural practices in the context of global climate change.

DOI: 10.33899/injes.v26i2.56079,

التقييم المكاني الزماني والتنبؤ بديناميكيات درجة حرارة سطح الأرض في كركوك باستخدام تقنيات نظم المعلومات الجغرافية

سمية فالح حسن[1]، مصطفى رعد حميد[2]، بناز اديب فتاح [3]، منتظر عيدي شريف[4]*

[1،3،4] قسم هندسة تقنيات المساحة، الكلية التقنية الهندسية كركوك، الجامعة التقنية الشمالية، الموصل، العراق.

[2] قسم الابنية المدرسية، مديرية تربية بابل، بابل، العراق.

معلومات الارشفة

تاريخ الاستلام: 20- نوفمبر- 2024

تاريخ المراجعة: 15- فبراير- 2025

تاريخ القبول: 19- مايو- 2025

تاريخ النشر الالكتروني: 01- ابريل- 2026

الكلمات المفتاحية:

درجة حرارة السطح،

مؤشر النباتات،

نظم المعلومات الجغرافية،

الغطاء النباتي.

المراسلة:

الاسم: منتظر عيدي شريف

Email: muntadher.a.shareef@ntu.edu.iq

الملخص

تعرضت منطقة كركوك في العراق لتهديدات بسبب الاحتباس الحراري والتغيرات المناخية وارتفاع درجات الحرارة على مدى العقود القليلة الماضية. تتناول هذه الدراسة التغيرات الزمانية والمكانية في درجة حرارة سطح الأرض (LST) وكيف تؤثر على الغطاء النباتي في كركوك، العراق، خلال فترة زمنية تمتد من 1 يناير 2019 إلى 31 ديسمبر 2019. باستخدام بيانات الأقمار الصناعية وتقنيات نظم المعلومات الجغرافية (GIS)، تم تحليل العلاقة بين (LST) ومؤشر الفرق النباتي المُطَبّع (NDVI)، حيث أظهرت النتائج وجود علاقة متوسطة وسلبية ($R^2 = 0.65$) بالإضافة إلى ذلك، أوضحت العلاقة بين (NDVI) وإنتاجية القمح في كركوك وجود ارتباط إيجابي قوي ($R^2 = 0.89$). وتشير النتائج إلى أن عوامل مثل التوسع الحضري، وتغير أنماط الزراعة، والتغيرات المناخية العالمية تسهم في ارتفاع (LST). وتؤكد هذه النتائج على أهمية استخدام أدوات الاستشعار عن بعد ونظم المعلومات الجغرافية لتقييم تأثيرات المناخ على الظروف البيئية، والتي تعد ضرورية لإدارة الأراضي والزراعة بشكل مستدام في ظل تغير المناخ العالمي.

DOI: 10.33899/injes.v26i2.56079, ©Authors, 2026, College of Science, University of Mosul.

Introduction

The Earth's surface temperature (LST) has risen as a result of global climate change, impacting vegetation regions, land use, land cover, water supplies, and other factors that contribute to a variety of environmental challenges (Mukherjee and Singh, 2020). LST is the term used to describe the temperature of the Earth's surface, including that of exposed soil, vegetation canopy, land use, land cover, etc. (Tahooni et al., 2023). The knowledge of several words that disrupt the energy balance at the surface is crucial for hydrologists, agronomists, and meteorologists (Taheri et al., 2022). Nonetheless, one of the crucial factors that affects the processes of hydrosphere-biosphere-atmosphere interaction is LST (Jia et al., 2022). LST is also utilized in a variety of fields, including vegetation cover, hydrological cycle, evapotranspiration, and climate change (Malik et al., 2019). It is the primary metric that is impacted by land surface features such as soil surface permeability, vegetation cover, land use, and vegetation type (Kabir et al., 2020). Numerous investigations have been carried out to track variations in LST brought on by variations in plant cover and land use. The majority of research has shown that vegetation cover and LST are inversely correlated, meaning that crop cover lowers LST (Kumar et al., 2012). Many scholars now investigate the connection between LST, NDVI, and land cover for land use by GIS and remote sensing techniques (Ahmed, 2014; Hasan et al., 2021; Hason et al., 2020). To track changes in the vegetative zone, a variety of plant cover indicators are available. However, one of the most popular, straightforward, and efficient indices is the NDVI (Lambin and Ehrlich, 1996). Using this indicator, changes in vegetation cover for any given area can be measured. Two sorts of methodologies, such as the standard

methodology and the remote sensing (RS) approach, can be utilized to assess LST (Green et al., 1994). In Shanghai, China, satellite data were utilized to ascertain the correlations between LST and NDVI, GIS and RS tools, which are shown to be useful in identifying the effects of climate change on the environment. The LST has changed significantly as a result of the quick changes in land use and land cover patterns (Sruthi and Aslam, 2015). Similar to Kirkuk in Iraq, where the area's plant cover was greatly impacted by LST increases (Aya and Kadhim, 2024; Mahmood and Ali, 2014). The vegetation cover in Kirkuk, Iraq, was greatly impacted by the rise in LST (Salahalden et al., 2024b).

The objective of the article is to examine the impact of increasing Land Surface Temperature (LST) due to global climate change, and how it affects land use, land cover, vegetation areas, and water resources, which are critical factors contributing to various environmental problems. The study seeks to explore the relationship between LST and vegetation indices such as NDVI, and the use of GIS and RS tools to monitor these relationships. Additionally, the article aims to present the case study of Kirkuk, Iraq, where rising LST has significantly affected vegetation cover, offering insights into the broader consequences of climate change on both local and global scales.

Materials and data acquisition

Study area

The City of Kirkuk is located in the northwest of Iraq. The study area is bordered by the Zagros Mountains to the north, the Hamrin Mountains to the south, the Lesser Zab Mountains to the west, and Al-Sulaymaniyah City to the east. Geographically, Kirkuk City is situated between latitudes 35 13′ and 36 29′ N and longitudes 44 00′ to 44 50′ E. The total area of this city is roughly 9,679 km^2 (Shareef et al., 2020). The distance from Baghdad, the capital of Iraq, is about 250 kilometers (Fig. 1). In the study area, the climate is semiarid and Mediterranean, with chilly winters and hot, dry summers (Jaber et al., 2022). Rainfall is minimal or nonexistent throughout the summer months, with the majority of precipitation falling between December and March (Stathi et al., 2023). Temperature plays a significant role in the climate, with peak temperatures reaching approximately 48 ℃ during summer and dropping to -1 ℃ in winter. The city of Kirkuk is located between 340 and 360 meters above sea level on the steep northern portion of the Kirkuk plain (Mohammed et al., 2024). The plain's eastern and northern borders are delineated by the Hamrin structure and the Lesser Zab River, while its western and northern borders are delineated by the Kirkuk structure (sometimes called the Baba Dome) and the Hamrin structure (Salahalden et al., 2024a).

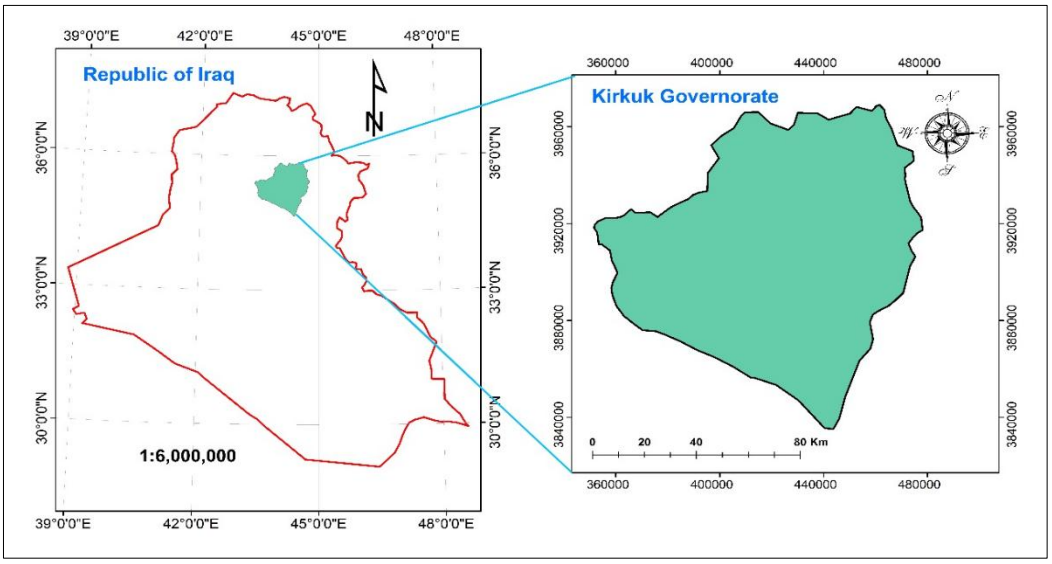

Fig. 1. Study area in Kirkuk City.

Data and pre-processing

Data used

The data used in this study are taken from the Landsat-8 multispectral sensor. Landsat-8 is officially launched on 11 February 2013, and is considered the eighth satellite in the series of Landsat family. It has a two-sensor aboard, including the Operational Land Imager (OLI) and the Thermal Infrared Sensor (TIRS), which are detailed in reference (Shen et al., 2021). The thermal sensor consists of two thermal bands: bands 10 and 11, which are generally used to provide the surface temperature with high accuracy and are collected at 100 meters. The thermal images include radiometric rescaling of the TIRS thermal to be used to extract the surface temperatures. In this study, we have used band 10 to extract the surface temperature; moreover, some of the Landsat-8 categories are illustrated in Table 1. All images were downloaded for free from the USGS Earth Explorer (https://earthexplorer.usgs.gov/) with a cloud coverage of less than 2%, for summer and winter seasons.

Table 1. Landsat-8 categories.

		Categories/ resolution (m)
Sensors	OLI (30-60m)	Band 1 to band 7 and band 9 with resolution 30 m, band 8 is 15 m,
	TIRS(100m)	Bands 10 and 11 are 100 m
Altitude		705 Km
Inclination		98.2
Orbit		Polar, sun-synchronous

Methods

In this article, ArcGIS, meteorological data, and ENVI software are used in order to determine the temperature changes in 2019 from January to December. The following flowchart (Figure 2) illustrates the procedure for the methodology.

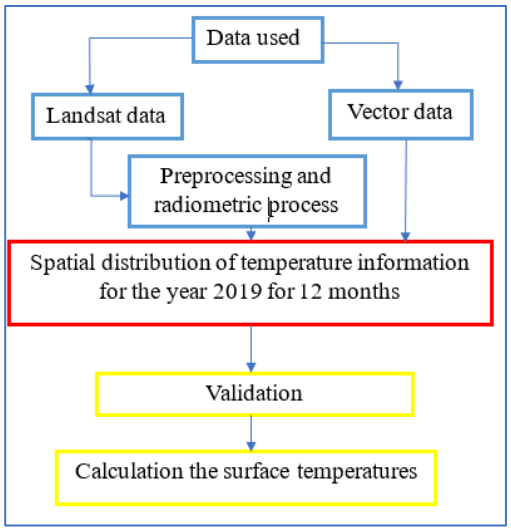

Fig. 2. Overall methodology.

Normalized Difference Vegetation Index (NDVI)

One of the most often used indices in vegetation remote sensing is the Normalized Difference Vegetation Index (NDVI), which was created by Rouse et al (1973). It uses the visible (0.45 to 0.67µm) and near-infrared (0.85 to 0.88µm) regions within the electromagnetic spectrum to assess remote sensing data and determine whether the target being detected consists of actual green plants. This index is used for various purposes, particularly those related to other ground characteristics such as the percentage of landscape cover, plant activity or season end, water surface, vegetation density, and biomass (Bagherzadeh et al., 2020).

Therefore, the NDVI is derived by concentrating on satellite bands like red and near-infrared that are most sensitive to vegetation. Next, observe how many of the rays that fall on the plant are absorbed and reflected. The majority of the visible light is generally absorbed by healthy plants. On the other hand, it reflects a lot of the near-infrared. In contrast, poor vegetation reflects a lot of visible light and a little amount of near-infrared light (Roznik et al., 2022). By subtracting the red reflectance values from the near-infrared, the NDVI algorithm divides the result by the sum of the red and near-infrared bands.

$$NDVI = (p_{NIR} - p_{red})/(p_{NIR} + p_{red}) \quad (1)$$

Where: p_{NIR} is the reflectance or radiance in a near infrared channel (0.78–0.90 µm TM/ETM+ and 0.72–1.1 µm AVHRR) and p_{red} is the reflectance or radiance in a visible channel (0.63–0.69 µm TM/ETM+ and 0.58–0.68 µm AVHRR)(Chen et al., 2016).

When applied to well-vegetated sites, NDVI readings, which are expressed as a ratio with a range of (-1 to +1), take on comparatively high values (0.3–0.6) (Chen et al., 2016). The determined NDVI values are often divided into two categories: non-vegetation (NDVI <0) and vegetation (NDVI >0), which includes deciduous and evergreen monsoon forests (water bodies, barren and rocky land). Consequently, apart from the capacity to distinguish between places that are vegetated and those that are not (e.g., bare soil and roads). Water and other land cover can be distinguished using the NDVI (Bhagat and Sonawane, 2011).

Radiometric Calibration of Landsat-8 data

This section's calibration procedure of Landsat-8 data will be used for the United States Geological Survey Earth Resources Observation and Science USGS EROS center's deliverables. In addition to the Thermal Infrared Sensor (TIRS), this product often includes the Operational Land Imager (OLI) as multispectral picture data, which is represented by quantizing and scaling digital numbers (DN) (Bhagat and Sonawane, 2011). The products come in 16-bit unsigned integer format, and the product metadata file contains radiometric rescaling coefficients that can be used to rescale them to the Top of Atmosphere (TOA) reflectance and/or radiance (MTL file). The thermal constants that were needed to convert the TIRS data to the at-satellite brightness temperature are also included in the MTL file. Therefore, calibrating picture data to radiance, reflectance, or brightness temperatures is the primary goal of radiometric calibration (Shamsuzzoha et al., 2021) and that, as shown in Figure 3, we will achieve in this section.

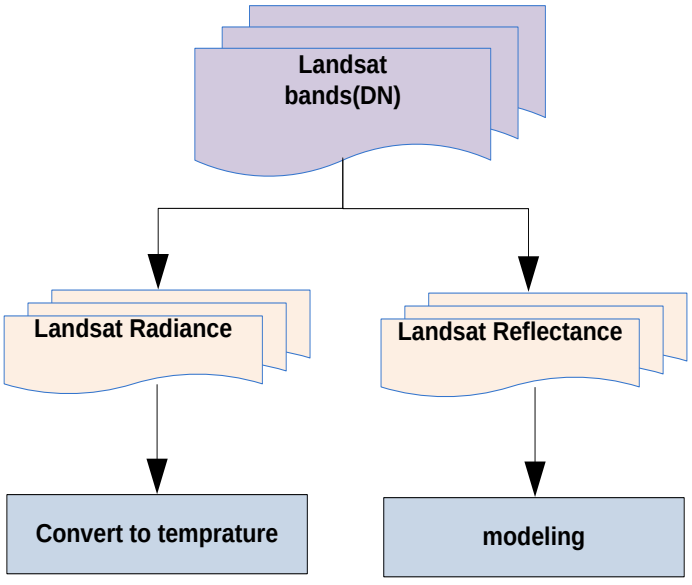

Fig. 3. Transformation from digital number to temperature.

Conversion to TOA Radiance

The energy in the form of a flux or irradiance can interact with a surface area in a certain direction and with a solid angle. This behaviour, which can be emitting, reflecting, transmitting, or receiving, is known as radiation. It is measured at the satellite sensor and is dependent on reflectance. However, for relatively obvious Landsat views, a decline in between-view instability could be accomplished by way of normalization to get solar irradiance by transforming (Markham et al., 2016). Spectral radiance at the sensor's space (L_λ) is certainly determined in [watts/ meter squared * ster * μm] also be computed as TOA spectral radiance directly from OLI as well as TIRS (thermal) band data using equation (2).

$$L_\lambda = M_L Q_{cal} + A_L \quad (2)$$

Where: L_λ = spectral radiance computed using TOA measured by {Watts/(m2 * srad * μm)}, and M_L = refers to specific band multiplicative rescaling factor provided in the metadata, AL = refers to specific band additive rescaling factor provided in image metadata as a form (RADIANCE ADD BAND-x), x = number of the band), Q_{cal} = calibrated and quantized digital number (DN).

This equation significantly depends on rescaling factors (Table 2), which are extracted from the metadata of Landsat-8 images.

Table 2: Spectral Radiance Range in {watts/ (meter squared * ster * μm)}.

Band Number	RADIANCE MULT BAND	RADIANCE ADD BAND
1	1.3325E-02	-66.62635
2	1.3588E-02	-67.94135
3	1.2442E-02	-62.21135
4	1.0538E-02	-52.68921
5	6.3945E-03	-31.97240
6	1.6111E-03	-8.05545
7	5.2408E-04	-2.62042
8	1.1870E-02	-59.35106
9	2.6278E-03	-13.13878
10	3.3420E-04	0.10000
11	3.3420E-04	0.10000

Conversion to Brightness Temperature

Using Plank's law, brightness temperatures -also referred to as blackbody temperatures - can be calculated from the radiances on TOA calculated by satellite TIR sensors. The assumption that the water vapor concentration of the atmosphere is constant for a relatively small area allows the atmospheric conditions to be considered uniform and ignores the influence of the atmosphere on the radiance temperature (Kleynhans et al., 2017). Consequently, the dispersion of the surface temperature fields can be reflected in the at-satellite brightness temperature. The water vapour content is known to fluctuate throughout time due to seasonality and internal variations in atmospheric conditions. It is inappropriate to compare the temperature shown by the satellite brightness temperature over many time periods (Chen et al., 2016). Equation (3) illustrates how TIRS Band data can be transformed from spectral radiance to brightness temperature using the thermal band constants included in the metadata file.

$$T_b = \frac{K_2}{ln\left(\frac{K_1}{L_\lambda} + 1\right)} \quad (3)$$

Where: T_b = brightness temperature from satellite, K_1 = Band-specific thermal conversion constant provided in the metadata, K_2 = Band-specific thermal conversion constant provided in the metadata. However, the temperature constants (K_1, K_2) are concerned to our data have been extracted from metadata file for thermal bands (band 10 and band 11) given in Table (2).

Table 2: Radiometric rescaling of TIRS thermal constants.

Band Number	K_1 CONSTANT	K_2 CONSTANT
10	774.89	1321.08
11	480.89	1201.14

Land Surface Temperature (LST)

The sparse and irregular distribution of weather observatories, the challenges associated with conducting field surveys, and the complicated nature of interpolating station data present obstacles to the continuous monitoring of harsh settings. Because of this, remotely sensed land surface temperature (LST) is very interesting for a range of biological and environmental applications (Abdulrahman et al., 2024). The radiative energy budget of the Earth's surface is determined by this important factor. Since it causes the turbulent heat exchanges and outgoing long-wavelength radiation at the interface between the land and atmosphere, the land surface temperature (LST) is a crucial input for land-surface models that analyse evapotranspiration, estimate soil moisture, and monitor dryness (Amer et al., 2023). Finally, the land surface temperature is calculated using equation (4).

$$L_{ST\square} = \frac{T_b}{1 + \left(\lambda + \frac{T_b}{p}\right) * ln(\varepsilon)} \quad (4)$$

Where: The typical value for emissivity ($\boldsymbol{\varepsilon}$) is 0.95 (Aya and Kadhim, 2024).

Results and discussion

Earth's surface temperature

The analysis of spatial and temporal variance in Land Surface Temperature (LST) for Kirkuk Governorate during the year 2019 reveals distinct differences between areas with vegetation or water bodies and those with urban or arid land. The Figures below show the results of the present study, which looked at the land surface temperature (LST) in the Kirkuk Governorate over time and space in 2019. It shows that the LST varied a lot between different types of land cover, especially between urban areas, dry lands, and areas with plants and water. These findings align with global studies on the relationship between LST, land use, and land cover, further reinforcing the cooling effects of vegetation and water compared to urbanized and barren landscapes.

In January, as shown in Figure 4, the satellite-derived LST ranged from 4.44°C to 15.34°C, while the measured air temperatures ranged from 13°C to 15.5°C. This indicates that while the satellite data provides a useful estimate of surface temperature, it tends to underestimate the actual conditions on the ground, especially in cooler months. This discrepancy becomes even more pronounced during the hotter months, suggesting potential atmospheric interference and limitations of remote sensing technologies in accurately capturing extreme temperatures.

In February, LST values ranged between 6.11°C and 16.11°C, while the measured temperatures were between 15°C and 17.5°C, maintaining a similar pattern of satellite data underestimating real-world conditions. March shows LST values between 10°C and 16.6°C, while ground temperatures ranged from 19°C to 21.5°C, as shown in Figure 4. As temperatures began to rise in spring, the gap between LST and measured temperatures became more evident, which could be attributed to increasing urban activity, a phenomenon commonly referred to as the Urban Heat Island (UHI) effect.

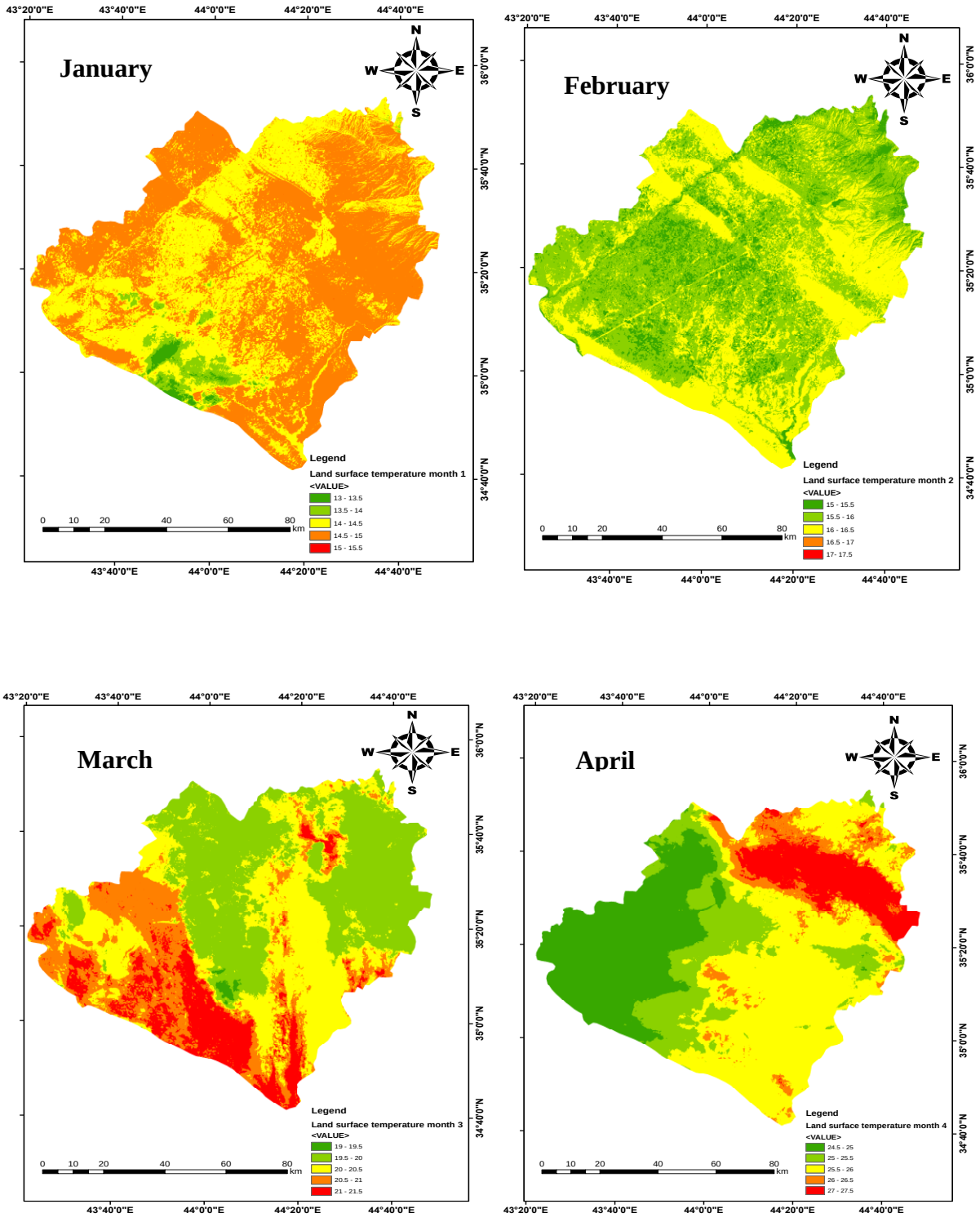

Fig. 4. Distribution of land surface temperature from January to April.

By April, the LST ranged from 17.2 °C to 19.1 °C, while the measured ground temperatures climbed to between 24.5 °C and 27.5 °C. In May, LST varied from 18.3 °C to 21.1 °C, but measured ground temperatures reached as high as 31.5 °C to 34°C. This month is critical as it marks the transition to summer, where the difference between LST and actual

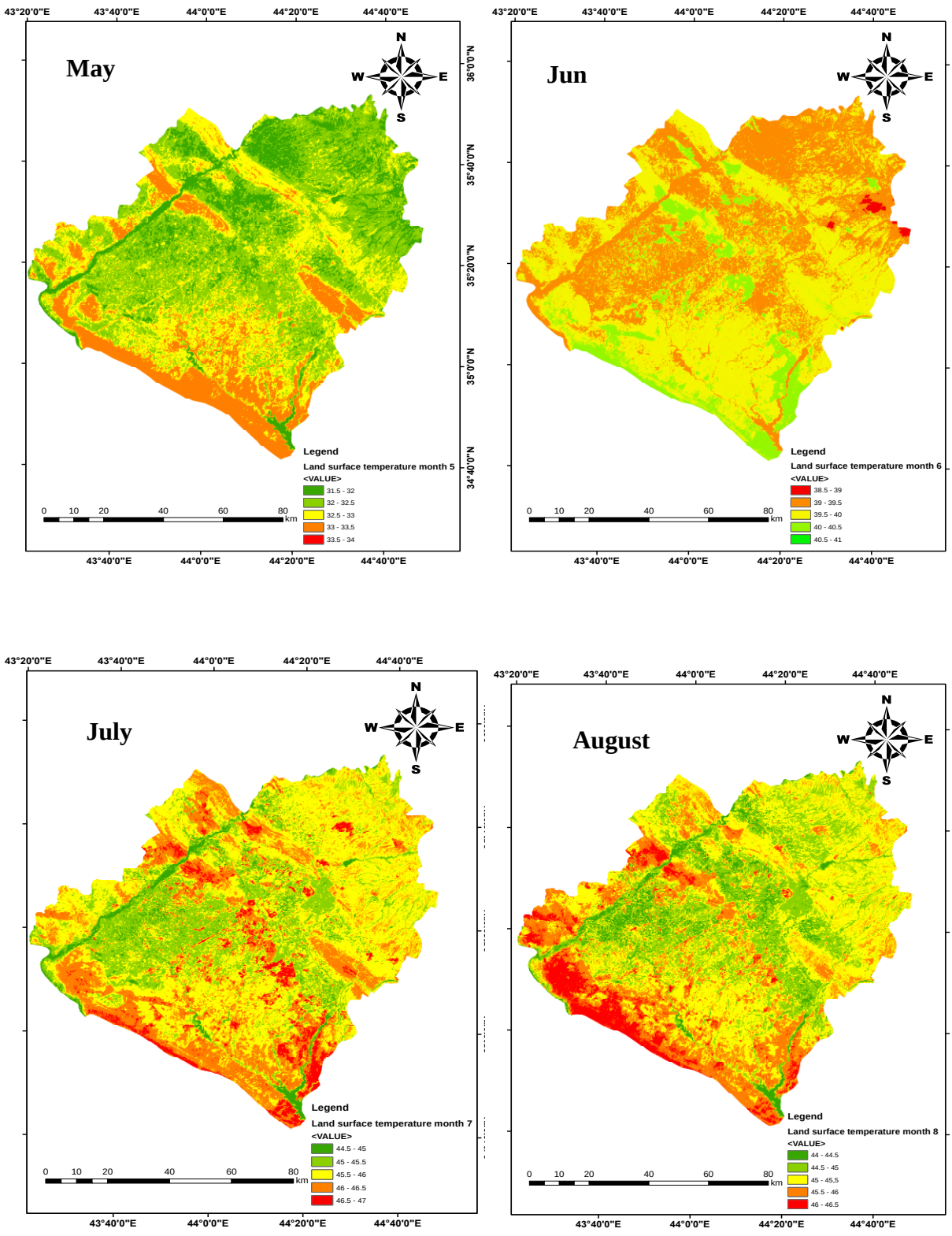

Fig. 5. Distribution of land surface temperature from May to August.

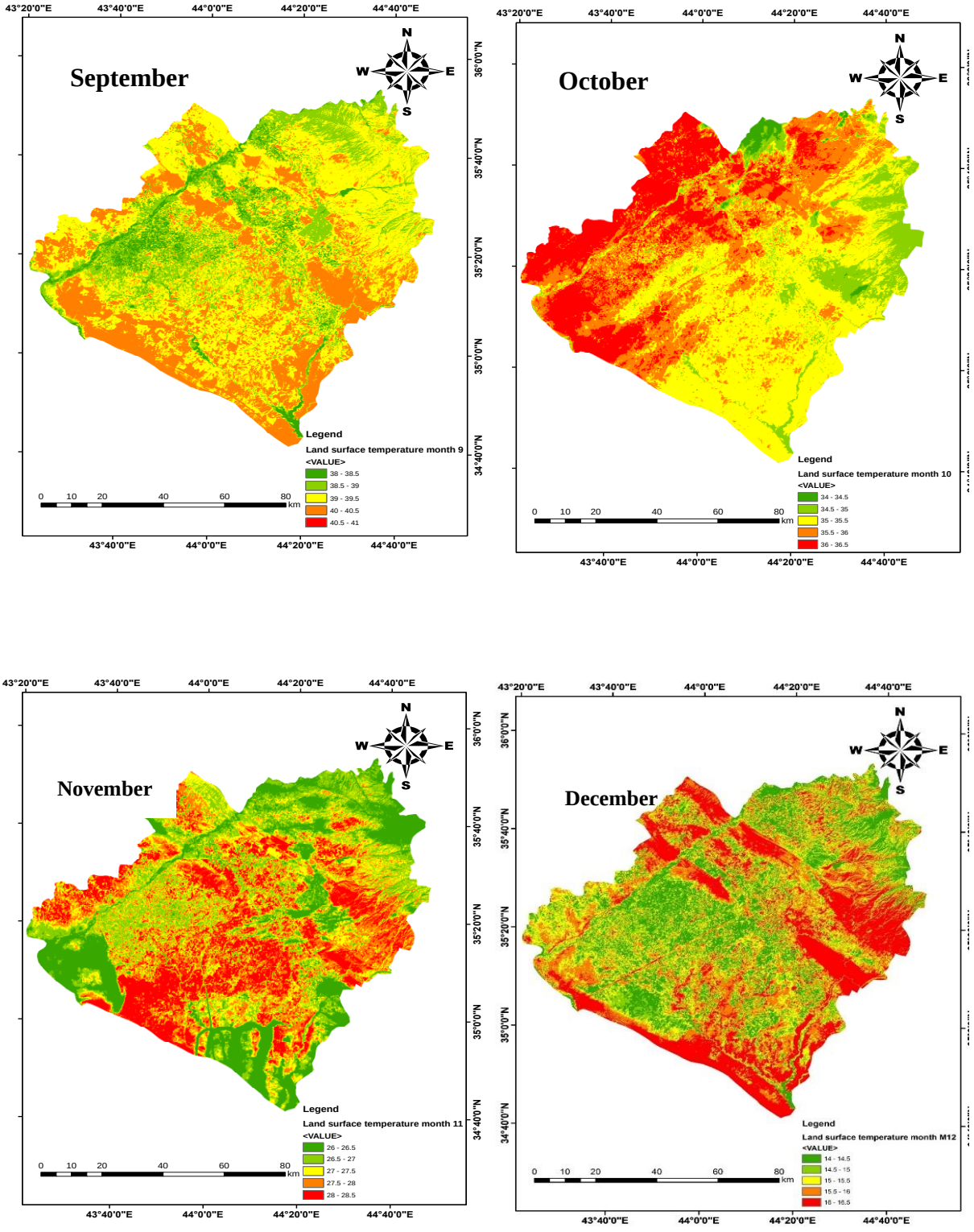

Fig. 6. Distribution of land surface temperature from September to December.

temperatures become even more pronounced (shown in Figure 4). For instance, in June, LST values ranged from 23.8°C to 25°C, while ground temperatures ranged from 38.5°C to 41°C. The highest divergence occurred in July and August, where satellite-derived LST ranged from 26.6°C to 29.4°C, but ground temperatures ranged from 44.5°C to 47°C in July and 44°C to 46.5°C in August (as shown in Figure 5).

In the latter half of the year, LST values begin to decrease, but still underestimate the actual measured temperatures. For instance, in September, the LST ranged from 26.1°C to 25°C, while ground measurements were recorded between 38°C and 41°C. Similarly, in October, LST values dropped to between 22.7°C and 20°C, while ground temperatures remained elevated, between 34°C and 36.5°C. In November and December, the gap between LST and measured temperatures becomes smaller again, with LST in November ranging from 15.5°C to 15°C, compared to measured temperatures of 26°C to 28.5°C. In December, LST values were recorded between 7.2°C and 6.1°C, while ground temperatures ranged from 14°C to 16.5°C, as shown in Figure 6.

The findings also underscore the impact of the UHI in the urban centre of Kirkuk, where higher LST values were recorded compared to surrounding rural areas. The dense built-up areas, concrete surfaces, and lack of greenery contribute to heat retention, exacerbating the UHI effect. In contrast, regions with significant vegetation cover and water bodies showed significantly lower LST values, supporting the cooling effects of evapotranspiration and the role of natural landscapes in temperature regulation.

Table 3: Land surface temperature ranges during the year with different areas.

Date	Land Surface Temperature												
	>15 °C		15-20 °C		20-25 °C		25-30 °C		>30 °C		Total	%	Average LST
	Area (m^2)	%	Area (m^2)	%	Area (m^2)	%	Area (m^2)	%	Area (m^2)	%			
2019/1/1	570	0.04	319627.2	24.46	771611	59.05	214390.4	16.41	511	0.04	1306710	100	22.10
2019/3/4	0	0.00	533633.6	40.84	621326	47.55	150589	11.52	1168	0.09	1306716.6	100	21.08
2019/6/7	3228	0.25	284694	21.79	695205	53.20	305309	23.36	18281	1.40	1306717	100	22.70
2019/8/5	123948	9.49	601129	46.00	455857	34.89	85484	6.54	31873	2.44	1298291	100	20.04
2019/10/3	3.96	0.00	254956	19.51	459033	35.13	523691	40.08	58343	4.46	1296027	100	23.99
2019/12/1	52	0.00	272896	20.88	525128	40.19	393385	30.11	115304	8.82	1306765	100	23.84

In summary, the results show a clear inverse relationship between LST and vegetation cover, with vegetation consistently mitigating surface temperatures. This highlights the importance of urban planning that incorporates green spaces and water features to alleviate the UHI effect. On the other hand, the UHI effect has a significant impact on LST, leading to higher temperatures in cities compared to rural areas. This occurs because urban environments are dominated by heat-absorbing materials like concrete, asphalt, and dense buildings, which retain heat and increase surface temperatures throughout the day and night.

One of the key findings is the inverse relationship between vegetation cover and LST. Areas with more greenery tend to have lower surface temperatures due to the cooling effects of shade and evapotranspiration. Plants release moisture into the air, which helps to lower temperatures and makes urban green spaces essential for reducing the UHI effect. Moreover, there is a strong connection between air temperature and land surface temperature (LST). When LST changes, it directly impacts the air temperature near the ground. The way they relate to each other can be described using either a simple linear equation or a more complex nonlinear equation, depending on various environmental and climate conditions.

Furthermore, the substantial difference between satellite-derived LST and measured temperatures suggests the need for improved remote sensing techniques or ground-based validation to ensure accurate temperature monitoring, particularly in extreme weather conditions. The increasing LST trends in Kirkuk due to global climate change further emphasize the necessity for proactive measures to combat rising temperatures and their environmental impacts. On average, there has been an increase of 1.74 °C in LST in the Indus delta over the past 27-year period, as shown in Table 2.

Variation in NDVI at different times in Kirkuk

The Kirkuk Governorate's NDVI indicator displays the time difference. It demonstrates that the greatest NDVI in 2019 was in January, with 0.725. This is because of the increase in the amount of rain. However, the seventh month of 2019 had the lowest NDVI, at 0.545. The

temporal change in the vegetation area is depicted by these NDVI measurements. In the figure, the brown color denotes water and arid regions with negative NDVI values, whereas the green color indicates positive NDVI values with green flora.

LST effect on vegetation

As seen in Figure (7), the correlation between LST and NDVI is used to evaluate the impact of LST on delta vegetation. With a coefficient of determination of R^2 = 0.65 and regression equation (5), it demonstrates a reasonable but unfavourable statistical link between NDVI and LST. Thus, as LST increased, NDVI decreased for the vegetation.

$$LST = -19.04 \times NDVI + 35 \qquad (5)$$

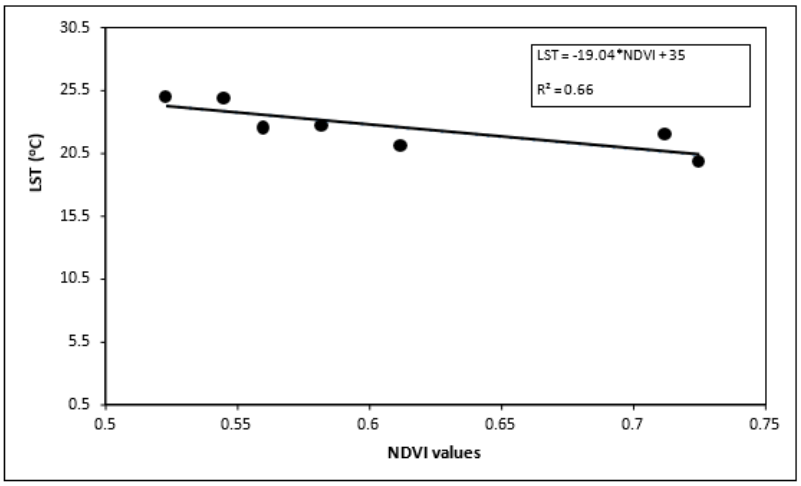

Fig.7. Relationship between NDVI and LST.

Conclusion

1. Land surface temperature (LST) in Kirkuk shows a significant variation throughout 2019, ranging from approximately 4.4°C in winter to over 46°C during peak summer months.
2. There is a clear inverse relationship between vegetation cover (measured by NDVI) and surface temperature, with greener areas exhibiting notably cooler temperatures due to natural shading and evapotranspiration.
3. Urban areas in Kirkuk experience significantly higher surface temperatures compared to rural and vegetated zones, demonstrating the urban heat island effect driven by dense construction and limited greenery.
4. Satellite-derived LST measurements tend to underestimate actual ground temperatures, especially during extreme heat, highlighting the need for complementary ground-based monitoring methods.
5. The increase in LST is influenced by urban expansion, changes in cropping patterns and global climate change, pointing to the importance of sustainable land use and urban planning.
6. The study underscores the need for integrating more green spaces and adopting adaptive land management strategies to mitigate heat effects and promote environmental sustainability in Kirkuk.

References

Abdulrahman, M.I., Shareef, M.A., and Al-Attar, A.A., 2024. Deep Learning (CNN) For Detecting Road Infrastructure in Old Mosul City Using High-Resolution Aerial Imagery. Baghdad Science Journal. https://doi.org/10.21123/bsj.2024.9449

Ahmed, K.A., 2014. Determination of Irrigated Field Units in North Al-Jazeera Irrigation Project Using Remote Sensing Data. Tikrit Journal of Engineering Sciences, 21, 68-74.

Amer, A., Al-Hadithi, M., and Shareef, M.A., 2023. Assessment Of Landslide Hazards Using GIS-Based Techniques: An Overview 2000-2020. NTU Journal of Renewable Energy, 4, 18-25. DOI:10.56286/ntujre.v4i1.407

Aya, M.R. and Kadhim, A.A., 2024. Land Surface Temperature Estimation from Landsat Thermal Infrared Imagery in Karbala, Iraq. Iraqi National Journal of Earth Science (INJES), DOI:10.33899/earth.2024.144879.1179

Bagherzadeh, A., Hoseini, A.V., and Totmaj, L.H., 2020. The Effects of Climate Change on Normalized Difference Vegetation Index (NDVI) in the Northeast of Iran. Modeling Earth Systems and Environment, 6, 671-683. DOI:10.1007/s40808-020-00724-x

Bhagat, V.S., and Sonawane, K.R., 2011. Use of Landsat ETM+ Data for Delineation Of Water Bodies in Hilly Zones. Journal of Hydroinformatics, 13, 661-671.

Chen, W., Zhang, Y., Gao, W., and Zhou, D., 2016. The Investigation of Urbanization and Urban Heat Island in Beijing Based on Remote Sensing. Procedia-Social and Behavioral Sciences, 216, 141-150.

Green, K., Kempka, D., and Lackey, L., 1994. Using Remote Sensing to Detect and Monitor Land-Cover and Land-Use Change. Photogrammetric Engineering and Remote Sensing, 60, 331-337.

Hasan, S.F., Shareef, M.A., and Hassan, N.D., 2021. Speckle Filtering Impact on Land Use/Land Cover Classification Area Using the Combination of Sentinel-1a and Sentinel-2b (A Case Study of Kirkuk City, Iraq). Arabian Journal of Geosciences, 14, 276.

Hason, M.M., Abbood, I.S., and Aldeen Odaa, S., 2020. Land Cover Reflectance of Iraqi Marshlands Based on Visible Spectral Multiband of Satellite Imagery. Results In Engineering, 8, 100167.

Jaber, H.S., Shareef, M.A., and Merzah, Z.F., 2022. Object-Based Approaches for Land Use-Land Cover Classification Using High Resolution Quick Bird Satellite Imagery (A Case Study: Kerbela, Iraq). Geodesy And Cartography, 48, 85–91-85–91.

Jia, T., Yang, K., Peng, Z., Tang, L., Duan, H., and Luo, Y., 2022. Review on the Change Trend, Attribution Analysis, Retrieval, Simulation, and Prediction of Lake Surface Water Temperature. IEEE Journal of Selected Topics in Applied Earth Observations and Remote Sensing, 15, 6324-6355. DOI:10.1109/JSTARS.2022.3188788

Kabir, E.B., Bashari, H., Bassiri, M., and Mosaddeghi, M.R., 2020. Effects Of Land-Use/Cover Change on Soil Hydraulic Properties and Pore Characteristics in a Semi-Arid Region of Central Iran. Soil and Tillage Research, 197, 104478.

Kleynhans, T., Montanaro, M., Gerace, A., and Kanan, C., 2017. Predicting Top-of-Atmosphere Thermal Radiance Using Merra-2 Atmospheric Data with Deep Learning. Remote Sensing, 9, 1133.

Kumar, K.S., Bhaskar, P.U., and Padmakumari, K., 2012. Estimation Of Land Surface Temperature to Study Urban Heat Island Effect Using Landsat ETM+ Image. International Journal of Engineering Science and Technology, 4, 771-778.

Lambin, E.F., and Ehrlich, D., 1996. The Surface Temperature-Vegetation Index Space for Land Cover and Land-Cover Change Analysis. International Journal of Remote Sensing, 17, 463-487.

Mahmood, F. and Ali, A., 2014. Using Remote Sensing Techniques to Assess Land Use/Land Cover Change in Laylan Sub-District, Kirkuk Province, Iraq. Iraqi Journal of Science, 55, 845-851.

Malik, M.S., Shukla, J.P., and Mishra, S., 2019. Relationship of LST, NDBI, and NDVI Using Landsat-8 Data in Kandaihimmat Watershed, Hoshangabad, India.

Markham, B. L., Arvidson, T., Barsi, J. A., Choate, M., Kaita, E., Levy, R., Lubke, M., and Masek, J. G. 2016. Landsat Program. Elsevier Reference Module in Earth Systems and Environmental Sciences.

Mohammed, P.A., Al Nuaimy, Q.A., and Shareef, M.A., 2024. Analyzing Soil Physical Properties in Kirkuk City, Iraq, Utilizing A Geographic Information System-Based Inverse Distance-Weighted Technique. Ecological Engineering and Environmental Technology (EEET), 25. DOI:10.12912/27197050/192346

Mukherjee, F., and Singh, D., 2020. Assessing Land Use–Land Cover Change and its Impact on Land Surface Temperature Using Landsat Data: A Comparison of Two Urban Areas in India. Earth Systems and Environment, 4, 385-407.

Roznik, M., Boyd, M., and Porth, L., 2022. Improving Crop Yield Estimation by Applying Higher Resolution Satellite NDVI Imagery and High-Resolution Cropland Masks. Remote Sensing Applications: Society and Environment, 25, 100693.

Salahalden, V., Shareef, M., and Al Nuaimy, Q., 2024a. Assessment of Deposited Red Clay Soil in Kirkuk City Using Remote Sensing Data and GIS Techniques. Nature Environment and Pollution Technology, 23. DOI:10.46488/NEPT.2024.v23i02.001

Salahalden, V.F., Shareef, M.A., and Al Nuaimy, Q.A., 2024b. Red Clay Soil Physical and Chemical Properties Distribution Using Remote Sensing and GIS Techniques in Kirkuk City, Iraq. The Iraqi Geological Journal, 194-220.

Shamsuzzoha, M., Noguchi, R., and Ahamed, T., 2021. Damaged Area Assessment of Cultivated Agricultural Lands Affected by Cyclone Bulbul in Coastal Region of Bangladesh Using Landsat 8 OLI and TIRS Datasets. Remote Sensing Applications: Society and Environment, 23, 100523.

Shareef, M., Hassan, N., Hasan, S., and Khenchaf, A., 2020. Integration of Sentinel-1a and Sentinel-2b Data for Land Use and Land Cover Mapping of the Kirkuk Governorate, Iraq. International Journal of Geoinformatics, 16.

Shen, Q., Wang, H., Shum, C., Jiang, L., Hsu, H., Gao, F., and Zhao, Y., 2021. Antarctic-Wide Annual Ice Flow Maps from Landsat 8 Imagery Between 2013 and 2019. International Journal of Digital Earth, 14, 597-618.

Sruthi, S., and Aslam, M.M., 2015. Agricultural Drought Analysis Using the NDVI and Land Surface Temperature Data: A Case Study of Raichur District. Aquatic Procedia, 4, 1258-1264.

Stathi, E., Kastridis, A., and Myronidis, D., 2023. Analysis of Hydrometeorological Characteristics and Water Demand in Semi-Arid Mediterranean Catchments Under Water Deficit Conditions. Climate, 11, 137. DOI:10.3390/cli11070137

Taheri, M., Mohammadian, A., Ganji, F., Bigdeli, M., and Nasseri, M., 2022. Energy-Based Approaches in Estimating Actual Evapotranspiration Focusing on Land Surface Temperature: A Review of Methods, Concepts, and Challenges. Energies, 15, 1264.

Tahooni, A., Kakroodi, A.A., and Kiavarz, M., 2023. Monitoring of Land Surface Albedo and its Impact on Land Surface Temperature (LST) Using Time Series of Remote Sensing Data. Ecological Informatics, 75, 102118. DOI:10.1016/j.ecoinf.2023.102118